



OPEN

Lanthanoid-containing polyoxometalate nanocatalysts in the synthesis of bioactive isatin-based compounds

Mansoureh Daraie¹, Masoud Mirzaei²✉, Maryam Bazargan², Vadjiheh Sadat Amiri^{2,3}, Bita Abdolahi Sanati^{2,3} & Majid M. Heravi¹✉

Lanthanoid-containing polyoxometalates (Ln-POMs) have been developed as effective and robust catalysts due to their Lewis acid–base active sites including the oxygen-enriched surfaces of POM and the unique 4f. electron configuration of Ln. As an extension of our interest in Ln-POMs, a series of as-synthesized nanocatalysts $K_{15}[Ln(BW_{11}O_{39})_2]$ (Ln-B₂W₂₂, Ln = La, Ce, Nd, Sm, Gd, and Er) synthesized and fully characterized using different techniques. The Ln³⁺ ion with a big ionic radius was chosen as the Lewis acid center which is sandwiched by two mono-lacunary Keggin [BW₁₁O₃₉]⁹⁻ units to form Ln-containing sandwiched type cluster. Consequently, the catalytic activity of nanocatalysts with different Ln was examined in the synthesis of bioactive isatin derivatives and compared under the same optimized reaction conditions in terms of yields of obtained products, indicating the superiority of the nano-Gd-B₂W₂₂ in the aforementioned simple one-pot reaction. The effects of different dosages of nanocatalyst, type of solvent, reaction time, and reaction temperature in this catalytic system were investigated and the best results were obtained in the presence of 10 mol% of nano-Gd-B₂W₂₂ in water for 12 min at the reflux condition.

The term “spiro” in organic chemistry was firstly defined by Von Baeyer in the late 1890s. This term is used when two hydrocarbon rings are assembled on a shared carbon atom which is named the spiro carbon atom. Presently, spiro organic structures are considered in designing new pharmaceuticals. The special biological and conformational characteristics with the complexity and rigidity properties of the spiro compounds, make them good chiral candidates in drug discovery^{1–4}.

Spirooxindole core is one of the most popular spiro compounds found in the structure of many alkaloids, bioactive synthetic compounds, and pharmaceuticals (Fig. 1)⁵. Spirooxindoles have shown various biological activities, including promising anticancer⁶, antimicrobial⁷, antiviral, antioxidant, anti-inflammatory, antileishmanial, and antiplasmodial agents^{8,9}. Moreover, some spirooxindole-based compounds have been developed as inhibitors of microtubule assembly, such as spirotryprostatin A, alstonisine, and ptopodind. According to the importance of spirooxindoles in drug discovery, many researches have been directed to find new efficient synthetic routes furnishing molecules containing this core^{10,11}.

Polyoxometalates (POMs), known as inorganic ligands, are discrete, anionic metal-oxide clusters of group V or VI transition metals in their highest oxidation state and exhibit a great diversity of sizes, nuclearities, and shapes^{12–14}. POMs benefit from interesting structural skeletons including protons (Brønsted acids, can promote acid-catalyzed reactions), oxygen atoms (with a high negative charge can be used in base-catalyzed reactions), and metal ions with unoccupied orbitals (Lewis acids)¹⁵. The motivation for choosing POMs comes not only from their intriguing structural diversity, but also they contain several potential applications in many fields such as sorbent^{16,17} catalysis^{18–20}, magnetic²¹, optical materials sensitive devices²², electro/photochromic systems²³, sensors²⁴ and medicine²⁵. Lacunary POMs are defect derivatives of saturated ones, including one or more vacant sites such as mono-lacunary, di, or tri-lacunary structures²⁶. The most common lacunary POMs are derivatives of the Keggin and Wells–Dawson ions, resulting frequently in sandwich-type clusters^{27,28}. Totally, structural vacancies in the lacunary POMs lead to enhance surface reactivity, therefore, they can be substituted by metals with strong Lewis acidity, such as lanthanoids or transition metals like zirconium to generate Lewis acid catalysts^{29,30}.

¹Department of Chemistry, School of Sciences, Alzahra University, Vanak, Tehran, Iran. ²Department of Chemistry, Faculty of Science, Ferdowsi University of Mashhad, 9177948974 Mashhad, Iran. ³ These authors contributed equally: Vadjiheh Sadat Amiri and Bita Abdolahi Sanati. ✉email: mirzaeesh@um.ac.ir; mmheravi@alzahra.ac.ir

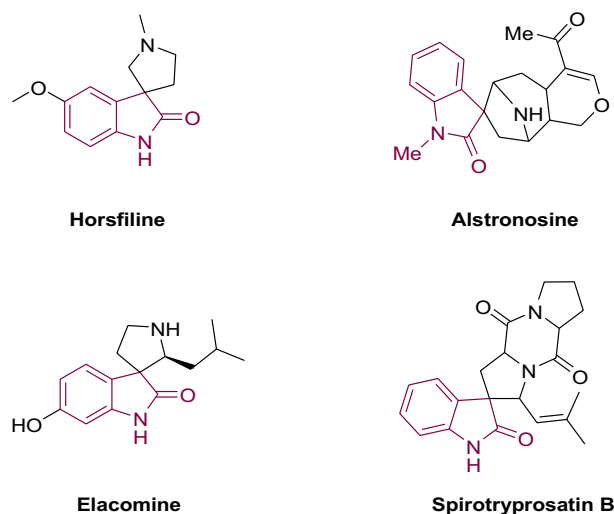


Figure 1. Selected spirooxindole natural products.

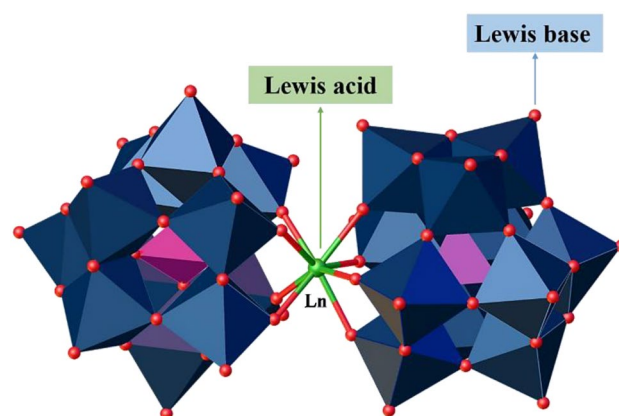


Figure 2. The structure of $\text{Ln-B}_2\text{W}_{22}$ nanocatalyst (Color code: W, dark blue; Ln, grey; O, red; B, purple). Reproduced from ref⁴⁰ with permission.

Lanthanoid-containing polyoxometalates (Ln-POMs), specially constructed from lacunary Keggin anions are structurally rigid clusters (Fig. 2) and showed higher stability, and have Lewis acid–base active sites compared with naked POMs. Also, a synergistic combination between the Ln and POM within one molecular structure can enhance their potential application in many fields such as luminescence, magnetism, and catalysis^{31,32}. Furthermore, due to their easy synthetic procedure and their robustness nature in the solid and solution, they can be also used in acid/base-catalyzed reactions for laboratory research purposes and industrial applications. Although there are several examples of isatin-based compounds synthesized using POMs or POMs-based composites^{33–36}, Lewis acid catalysts containing Ln-POMs have rarely been studied for them.

Herein, we have successfully synthesized a series of isostructural α -Keggin borotungstate dimers with Ln cations, $[\text{Ln}(\text{B}_2\text{W}_{22})_2]^{15-}$ ($\text{Ln-B}_2\text{W}_{22}$, Ln = La, Ce, Nd, Sm, Gd, and Er). Then, the related nanocatalysts were prepared by the top-down approach using the ultrasonic technique. In continuation of our efforts towards advancing synthetic methods to achieve spirooxindoles, in this research, we want to introduce a highly efficient, environmentally benign, and simple one-pot method for the nano- $\text{Gd-B}_2\text{W}_{22}$ -catalyzed synthesis of bioactive spirooxindole derivatives^{37–39}.

Experimental

Chemicals and materials. The chemical compounds were purchased from Merck (Darmstadt, Germany, www.merckmillipore.com) and Sigma-Aldrich (St. Louis, MO, USA, www.sigmaaldrich.com) and used with no crystallization or purification.

Instrumentation. Electrothermal 9200 apparatus was employed to determine the melting point of products. Bruker Tensor 27 FT-IR spectrometer (400–4000 cm^{-1} region) was used to detect absorbance bands of organic products using a KBr disk containing the compounds. ^1H NMR, ^{13}C NMR spectra were recorded on a

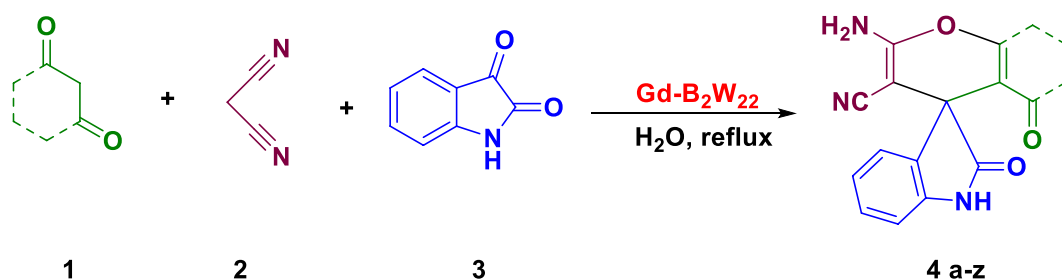


Figure 3. Synthesis of spiro-2-amino-4H-pryans.

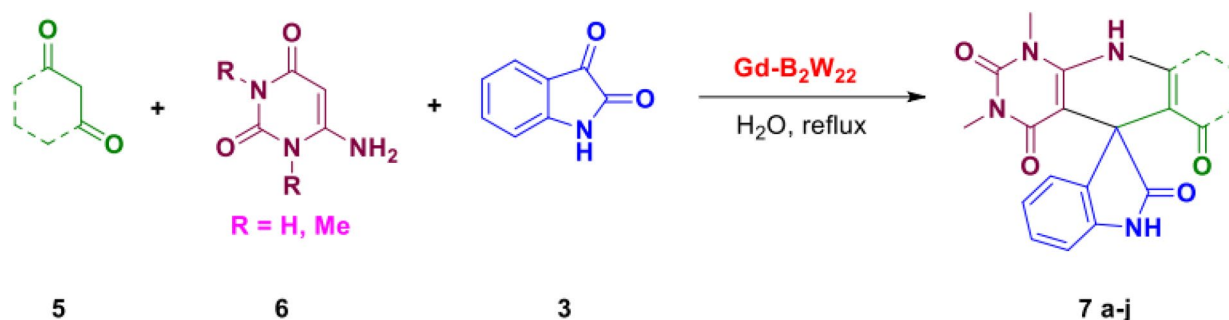


Figure 4. Synthesis of uracil-fused spirooxindoles.

Bruker AQS 400-AVANCE spectrometer at 400 and 100 MHz, respectively, using TMS as an internal standard (DMSO solution). Also, the infrared spectra of catalysts were recorded in the range of 4000–400 cm^{-1} on a Thermo Nicolet/AVATAR 370 Elemental analysis (CHN) was performed using a Thermo Finnigan Flash EA 1112 microanalyzer. Metal content was measured by the Spectro Arcos ICP-OES spectrometer model 76004555 using in the range of 130–770 nm for ICP spectra. Powder X-ray diffraction (PXRD) data were collected on ASENWARE/AW-XDM300 X-ray powder diffractometer using $\text{Cu K}\alpha$ ($\lambda = 1.54184 \text{ \AA}$) radiation at room temperature with the scan range $2\theta = 3$ to 40° and step size of 0.05° and step time of 1 s. The scanning electron microscope (SEM) analysis, EDS, and EDS mapping were recorded using LEO-1450 VP at an acceleration voltage of 10.00 kV and resolution of about 500 nm (Zeiss, Germany).

Preparation of catalysts. The mono-lacunary Keggin $\text{K}_9[\text{BW}_{11}\text{O}_{39}]\cdot 13\text{H}_2\text{O}$ was synthesized according to a literature method and identified by FT-IR and elemental analysis⁴¹. Then, mono-lacunary Keggin can be stabilized by lanthanide centers in solution and in the solid-state to form sandwich-type polyoxometalates $\text{K}_{15}[\text{Ln}(\text{BW}_{11}\text{O}_{39})_2]\cdot n\text{H}_2\text{O}$ ($\text{Ln-B}_2\text{W}_{22}$, Ln = La, Ce, Nd, Sm, Gd, and Er)^{40,42}.

General synthetic procedure for catalysts. A mixture of lanthanoid nitrate (0.085 mmol) and $\text{K}_9[\text{BW}_{11}\text{O}_{39}]\cdot 13\text{H}_2\text{O}$ (0.155 mmol) in 20 mL of KCl (1 M) was stirred for 10 min in air and then the pH was adjusted to 5.0 by dropwise addition of 0.1 M KOH. The resulted mixture was stirred for a further 40 min at 50°C . Pure crystals of the catalysts were obtained by slow evaporation of the solvent after several days.

Synthesis of nanocatalysts. The mixture solution of Ethanol (10 mL), water (15 mL), and $\text{Ln-B}_2\text{W}_{22}$ crystals (0.03 g) were subjected to ultrasonication (150 W). After 20 min, nanocatalysts were collected by the centrifuge and then washed with cold water ($3 \times 5 \text{ mL}$) under vacuum. FT-IR spectra (KBr pellet, cm^{-1}) of nano- $\text{Ln-B}_2\text{W}_{22}$ were consistent with their spectra before doing the nano procedure (Fig. S2).

General procedure for the synthesis of spiro-2-amino-4H-pryans. A combination of 1,3-diketone, carbonyl compound (either isatin or acenaphthoquinone), α -cyano compound (either malononitrile or ethyl cyanoacetate), and $\text{Gd-B}_2\text{W}_{22}$ was stirred in water at ambient temperature until the complete formation of the product was traced by TLC (Fig. 3). Then, the crude product was filtered, washed with water and dissolved in hot ethanol for crystallization. Furthermore, all products were characterized and analyzed by melting points and FT-IR spectra, and the results were compared with those reported in the literature to prove the formation of target products.

General procedure for the synthesis of uracil fused spirooxindoles. A combination of isatin, uracil derivative (either 1,3-dimethyl-6-aminouracil or 6-aminouracil), 1,3-diketone compounds, and $\text{Gd-B}_2\text{W}_{22}$ was stirred in refluxing water for 8–26 min (Fig. 4). Then, the mixture was filtered, washed well with water and dried at 80°C . The product was recrystallized for further purification in hot ethanol. All products were characterized by melting point and the characterizations were compared with that of in literature.

Synthesis of pyrroloacridine derivatives. A mixture of isatin, aniline, dimedone and nanocatalyst was refluxed in water for an appropriate time (Fig. 5). By the completion of the reaction, the mixture was cooled down and filtered. Then the crude product was washed well with hot water, and finally crystallized in hot EtOH. The characterization data of products were compared with that published in the literature.

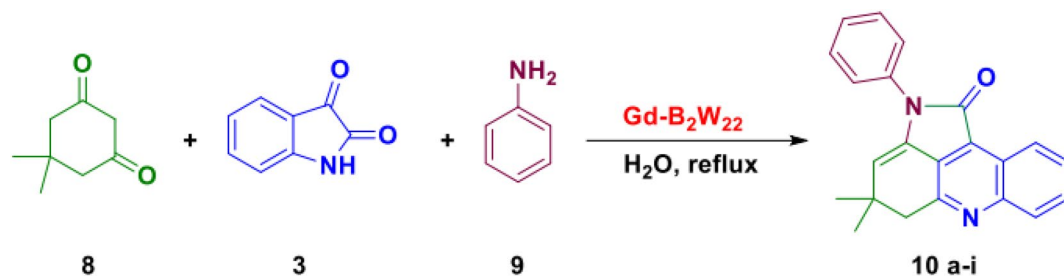


Figure 5. Synthesis of pyrroloacridine derivatives.

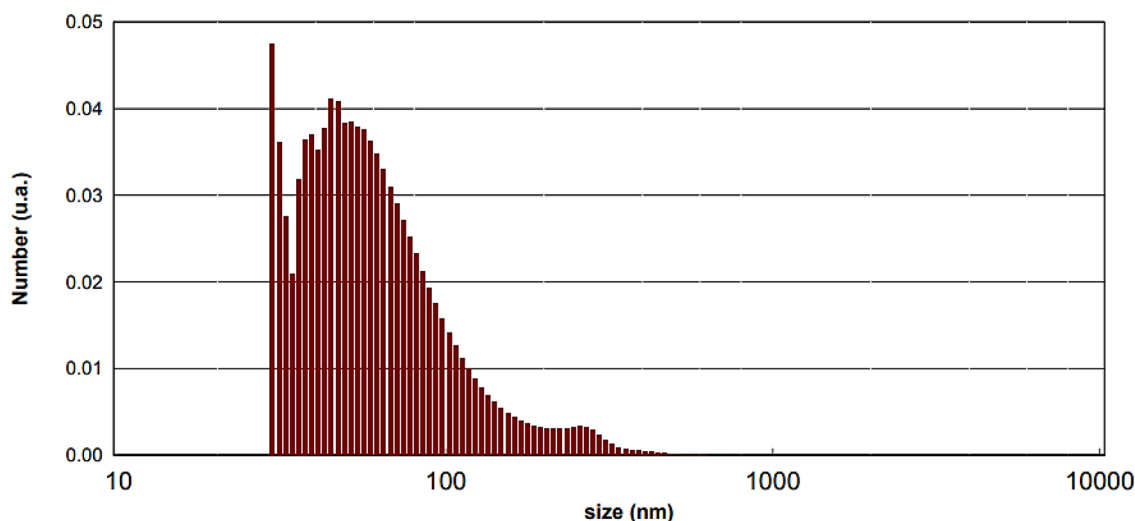


Figure 6. Particle size distribution histogram of nano-Gd-B₂W₂₂.

Characterization data. Spectral data for catalyst:

La-B₂W₂₂. Colorless needle-like crystals in 52.6% yield (based on W). Anal. Calcd. for H₅₂O₁₀₄LaK₁₅B₂W₂₂: K, 9.01; W, 65.2; La, 2.13; B, 0.33; H, 0.81%. Found: K, 9.37; W, 63.66; La, 2.38; B, 0.31; H, 0.77%. FT-IR (KBr pellet, cm⁻¹): 3451, 1616, 1254, 997, 948, 887, 832, 777, 521.

Ce-B₂W₂₂. Orange needle-like crystals in 55% yield (based on W). Anal. Calcd. for H₅₈O₁₀₇CeK₁₅B₂W₂₂: K, 8.94; W, 61.62; Ce, 2.13; B, 0.33; H, 0.89%. Found: K, 9.21; W, 60.75; Ce, 2.09; B, 0.31; H, 0.92%. FT-IR (KBr pellet, cm⁻¹): 3446, 1616, 1252, 996, 947, 887, 831, 777, 522.

Nd-B₂W₂₂. Light purple needle-like crystals in 49% yield (based on W). Anal. Calcd. for H₅₀O₁₀₃NdK₁₅B₂W₂₂: K, 9.03; W, 62.27; Nd, 2.22; B, 0.33; H, 0.78%. Found: K, 9.32; W, 63.41; Nd, 2.18; B, 0.31; H, 0.81%. FT-IR (KBr pellet, cm⁻¹): 3441, 1617, 1243, 996, 984, 885, 832, 777, 520.

Sm-B₂W₂₂. Colorless needle-like crystals in 62% yield (based on W). Anal. Calcd. for H₅₀O₁₀₃SmK₁₅B₂W₂₂: K, 9.02; W, 62.21; Sm, 2.31; B, 0.33; H, 0.78%. Found: K, 9.06; W, 63.41; Sm, 2.21; B, 0.31; H, 0.76%. FT-IR (KBr pellet, cm⁻¹): 3438, 2917, 1611, 1253, 1000, 494, 884, 831, 778, 519.

Gd-B₂W₂₂. Colorless needle-like crystals in 65% yield (based on W). Anal. Calcd. for H₆₀O₁₀₈GdK₁₅B₂W₂₂: K, 8.89; W, 61.30; Gd, 2.38; B, 0.33; H, 0.92%. Found: K, 9.01; W, 61.45; Gd, 2.31; B, 0.31; H, 98%. FT-IR (KBr pellet, cm⁻¹): 3471, 1611, 1253, 1000, 948, 883, 832, 799, 517.

Er-B₂W₂₂. Colorless needle-like crystals in 53% yield (based on W). Anal. Calcd. for H₅₂O₁₀₄ErK₁₅B₂W₂₂: K, 8.97; W, 61.88; Er, 2.56; B, 0.33; H, 0.80%. Found: K, 9.03; W, 61.51; Er, 2.51; B, 0.32; H, 0.91%. FT-IR (KBr pellet, cm⁻¹): 3428, 1621, 1258, 997, 948, 886, 835, 780, 522.

Results and discussion

Characterization of catalysts. Firstly, six lanthanoid-containing polyoxometalate K₁₅[Ln(BW₁₁O₃₉)₂] (Ln = La, Ce, Nd, Sm, Gd, and Er) crystals (microscopic size) of this study were obtained by reaction of the lanthanoid ion with the mono-lacunary Keggin [BW₁₁O₃₉]⁹⁻ at pH 5 (Figs. 2 and S3). Next, the above crystals were solved and subjected to ultrasonication and then nanocatalysts were collected by the centrifuge (top-down approach). The distribution histograms reveal that the average particle size of catalysts is less than 100 nm upon 20 min of sonication (Fig. 6). Particle size distribution histogram of other nanocatalysts are given in the Supplementary Figs. S4–S8.

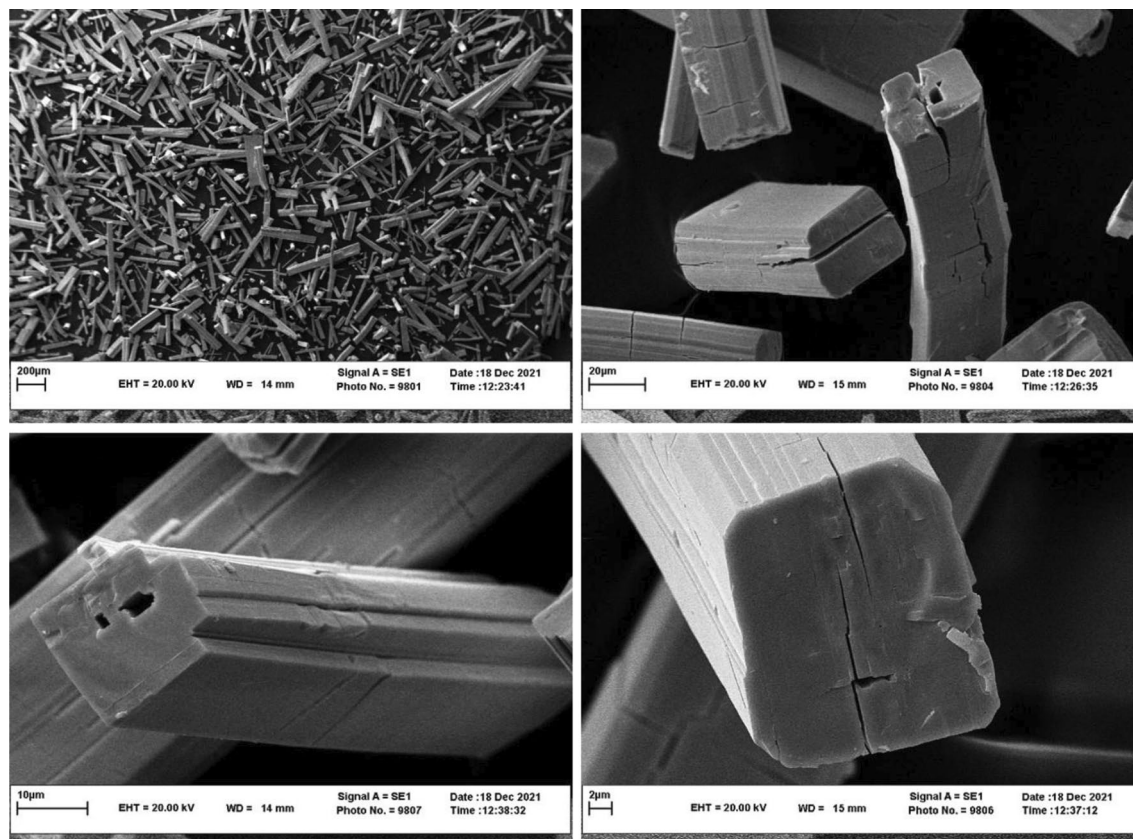


Figure 7. SEM images of nano-Gd-B₂W₂₂.

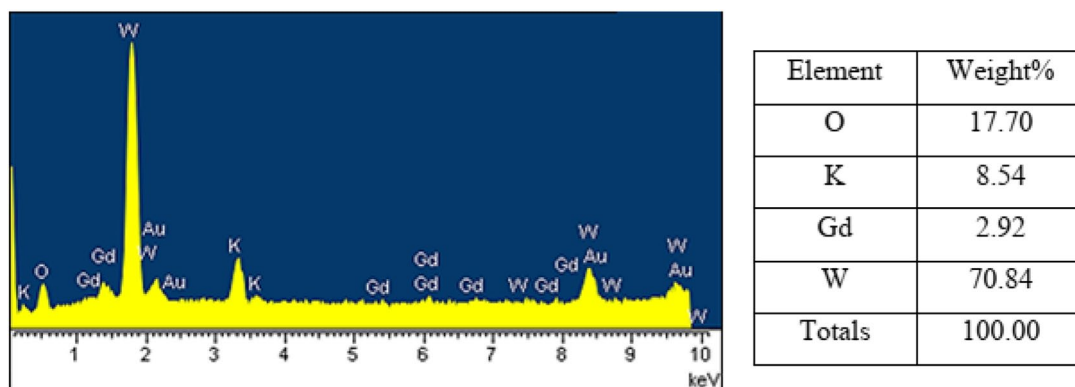


Figure 8. EDS spectrum of nano-Gd-B₂W₂₂.

Also, the SEM showed that the dominant morphology for nanocatalysts is rod-like (Fig. 7). Furthermore, the presence of O, K, Gd, and W in the nanocatalysts is confirmed by the EDS spectrum (Fig. 8). SEM images of La-B₂W₂₂ and EDS spectra of other nanocatalysts are given in Supplementary Information (Figs. S9–S14).

It is important to note that infrared spectroscopy is frequently employed technique for the characterization of POMs due to their characteristic metal–oxygen stretching vibrations that occur in the region between 400 and 1000 cm⁻¹ which is known as the fingerprint region for the POMs. As shown in Figs. S1, S2, and Table 1, the overlaid IR spectra strongly suggest the same structural family for all crystalline and nano compounds. Also, the IR spectra of catalysts present a similar vibration pattern with the mono-lacunary Keggin [BW₁₁O₃₉]⁹⁻, confirming the presence of the [BW₁₁O₃₉]⁹⁻ moiety in all compounds. Briefly, nano-Gd-B₂W₂₂ showed the absorption bands at 1610 and 3471 cm⁻¹ which attributed to the water molecules. The band at around 1250 cm⁻¹ is attributed for bending frequencies of O–B–O. Also, characteristic bands of the terminal oxygens ν_{as}(W–O_t) at 948 cm⁻¹ showed a red shift in comparison with the naked [BW₁₁O₃₉]⁹⁻ (995 cm⁻¹) that indicated [BW₁₁O₃₉]⁹⁻ anions coordinated to Ln³⁺ center (Fig. 9).

Also, the powder XRD pattern of the catalysts appears at around 9–10° for a 2θ value (similar to other mono-lacunary Keggin anions)⁴³ (Supplementary Fig. S15).

Compound	$\nu_{as}(B-O_B)$	$\nu_s(B-O_B)$	$\nu(W-O_B)$	$\nu_{as}(W-O_B)$	$\nu_{as}(W-O_B)$ and $\nu_{as}(W-O_C)$
La-B ₂ W ₂₂	997	521	887	948	832, 777
Ce-B ₂ W ₂₂	996	522	887	947	831, 777
Nd-B ₂ W ₂₂	996	520	885	948	832, 777
Sm-B ₂ W ₂₂	1000	519	884	949	831, 778
Gd-B ₂ W ₂₂	1000	517	883	948	832, 779
Er-B ₂ W ₂₂	997	522	886	948	835, 780
Naked BW ₁₁	995	515	889	954	836, 753

Table 1. Representation of important absorption bands (cm⁻¹) for K₁₅[Ln(BW₁₁O₃₉)₂] (Ln = La, Ce, Nd, Sm, Gd, and Er) and naked [BW₁₁O₃₉]⁹⁻ for comparison.

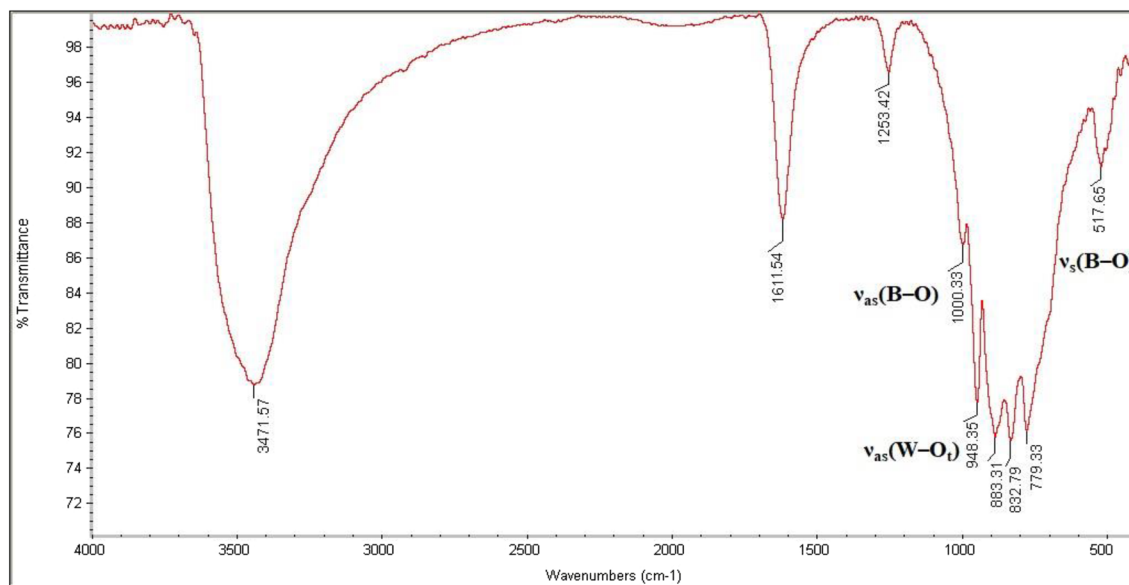


Figure 9. FTIR spectrum of nano-Gd-B₂W₂₂.

Catalytic activity. Ensuing this research, the catalytic activity of nano-Ln-B₂W₂₂ catalysts was tested in the model three-component reaction of isatin, malononitrile, and dimedone. To achieve eco-friendly optimized conditions, various factors were investigated. Initially, acidic catalysts including SSA, p-TSA, H₃PW₁₂O₄₀, Lanthanum nitrate, K₉[BW₁₁O₃₉]₁₃H₂O and ZnO were chosen to compare the results obtained by catalysts (Table 2). The Gd-B₂W₂₂ nanocatalyst was selected for further tests. Next, the effect of solvent was studied by running the model reaction in polar and non-polar solvents. Finally, the amount of catalyst was optimized to achieve the highest amount of product. The reaction was also repeated with no catalyst furnishing trace amount of product. That's while in the presence of 10 mol% of nanocatalyst, the target product was obtained in 96%. Therefore, ensuring by the effect of a catalyst in this reaction, the generalization was accomplished in water, in the presence of 10 mol% nano-Gd-B₂W₂₂ at reflux condition. It is important to note that the Lewis acidity (Z/r^3 ; Z = charge and r = ionic radius) of lanthanoids decreases with an increase in the ionic radii⁴⁴. However, among the Ln-B₂W₂₂ (Ln = La, Ce, Nd, Sm, Gd, and Er) catalysts examined, Gd-B₂W₂₂ showed better catalytic performance because by reducing the size from Gd to Er, the Er center was sterically hindered by two BW₁₁ ligands and its Lewis acid site is not well accessible.

The one-pot reaction of isatin, α -cyano compound (either malononitrile or ethylcyanoacetate), and 1,3-diketone (either ethyl acetoacetate, dimedone, or barbituric acid) or 3-methyl-1H-pyrazol-5(4H)-one/ 4-hydroxycoumarin or α -naphthol/ β -naphthol) gave the favorite products. Notwithstanding, the effect of substituent on isatin ring, the yield of products was found in good to high. By employing acenaphthenequinone instead of isatin, the expected spiro-4H-pyrans were formed in good to high yields. The products obtained from ethylcyanoacetate need a longer reaction time than those obtained from malononitrile that possibly is due to the lower reactivity of ethylcyanoacetate (Table 3). All products were known and identified by comparing their melting points with authentic literature. Some selected NMR spectra are presented in supplementary file (Figs. S16–S47).

In Scheme 1, we propose a sensible mechanism for the preparation of spirooxindole derivatives. First, the Gd-B₂W₂₂ catalyst, as a Lewis acid, activates the carbonyl group of the isatin molecule, and then malononitrile, due to α -activated hydrogens, will have a nucleophilic attack on activated carbon, which produces intermediate

Entry	Catalyst/amount (mol%)	Solvent	Temp. (°C)	Time (min)	Yield (%)
1	–	H ₂ O	Reflux	70	20
2	Silica sulfuric acid	H ₂ O	Reflux	50	80
3	p-Toluenesulfonic acid	H ₂ O	Reflux	45	82
4	H ₃ PW ₁₂ O ₄₀	H ₂ O	Reflux	40	88
5	Lanthanum nitrate	H ₂ O	Reflux	25	91
6	K ₉ [BW ₁₁ O ₃₉].13H ₂ O	H ₂ O	Reflux	20	90
7	ZnO	H ₂ O	Reflux	30	91
8	Nd-B ₂ W ₂₂ /10	H ₂ O	Reflux	20	90
9	Sm-B ₂ W ₂₂ /10	H ₂ O	Reflux	15	95
10	Er-B ₂ W ₂₂ /10	H ₂ O	Reflux	15	94
11	Ce-B ₂ W ₂₂ /10	H ₂ O	Reflux	25	92
12	La-B ₂ W ₂₂ /10	H ₂ O	Reflux	25	90
13	Gd-B ₂ W ₂₂ /10	H ₂ O	Reflux	12	96
14	Gd-B ₂ W ₂₂ /15	H ₂ O	Reflux	12	95
15	Gd-B ₂ W ₂₂ /10	H ₂ O	r.t	25	80
16	Gd-B ₂ W ₂₂ /10	H ₂ O	50 °C	20	91
17	Gd-B ₂ W ₂₂ /10	H ₂ O/EtOH	Reflux	15	90
18	Gd-B ₂ W ₂₂ /10	EtOH	Reflux	20	92
19	Gd-B ₂ W ₂₂ /10	CH ₂ Cl ₂	Reflux	25	90
20	Gd-B ₂ W ₂₂ /10	CH ₃ CN	Reflux	25	85
21	Gd-B ₂ W ₂₂ /10	Toluene	Reflux	30	85

Table 2. Optimization of the reaction conditions.

1. This intermediate creates intermediate 2 by elimination of water, and finally the corresponding product was synthesized by adding dimedone to this intermediate.

To confirm the wide effectiveness of nano-Gd-B₂W₂₂ as a catalyst, this was used in the reaction of isatin derivatives, 6-amino-1,3-dimethyl uracil, and 1,3-diketone (either dimedone, 1,3dimethyl barbituric acid, or barbituric acid). These reactions were successfully catalyzed by nano-Gd-B₂W₂₂ in refluxing water under optimized conditions furnishing spiro-products in good efficiency. The results are summarized in Table 4.

Next, the catalytic effect of nano-Gd-B₂W₂₂ was studied in the production of pyrroloacridine compounds through the one-pot reaction of isatin, aromatic amines, and dimedone. The generalization of this reaction was considered using different aromatic amine-bearing electron-donating and electron-withdrawing substituents. The expected pyrroloacridine derivatives were formed in wonderful yield within short reaction times as summarized in Table 5 (Fig. 10).

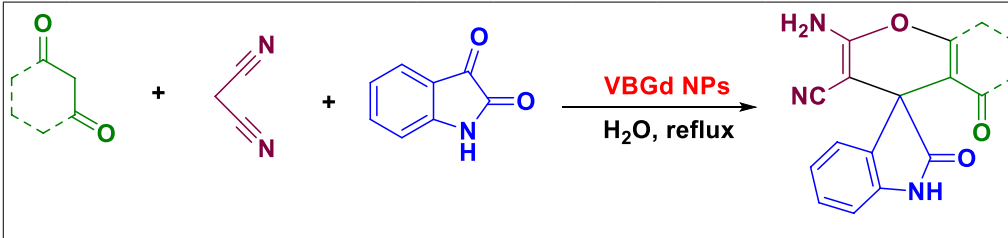
Entry	Product	Time (min)	Yield %	TOF	M.p./ °C Obs	M.p. °C/Lit
1		12	96	320	295–298	298–299
2		15	96	256	251–254	253–255
3		8	94	482	290–293	290–292
4		10	92	368	255–258	256–258
5		16	92	230	299–302	> 300
Continued						

Entry	Product	Time (min)	Yield %	TOF	M.p./ °C Obs	M.p. °C/Lit
6		20	91	182	253–254	251–253
7		22	90	163	241–243	240–242
8		25	90	144	261–263	262–264
9		20	91	182	270–272	273–275
10		25	90	144	208–211	207–209
Continued						

Entry	Product	Time (min)	Yield %	TOF	M.p./ °C Obs	M.p. °C/Lit
11		20	94	188	236–239	236–237
12		22	90	163	232–235	235–236
13		22	91	165	286–287	285–286
14		21	92	175	280–282	280–281
15		22	89	164	239–242	242–243
16		16	91	233	245–248	245–247
Continued						

Entry	Product	Time (min)	Yield %	TOF	M.p./ °C Obs	M.p. °C/Lit
17		10	95	395	269–273	268–270
18		14	92	262	257–260	259–262
19		18	93	206	> 300	> 300
20		24	88	146	195–198	194–196
21		26	91	141	> 300	> 300

Continued



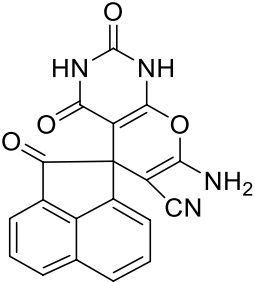
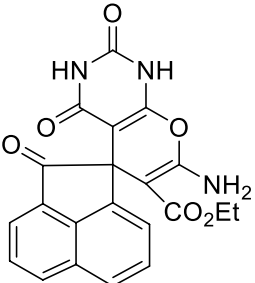
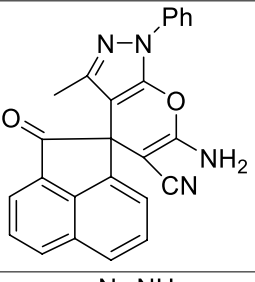
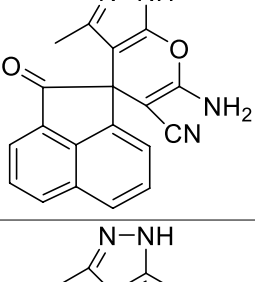
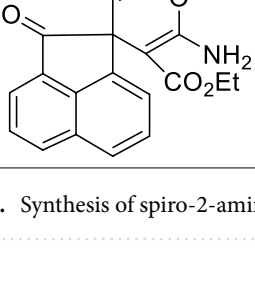
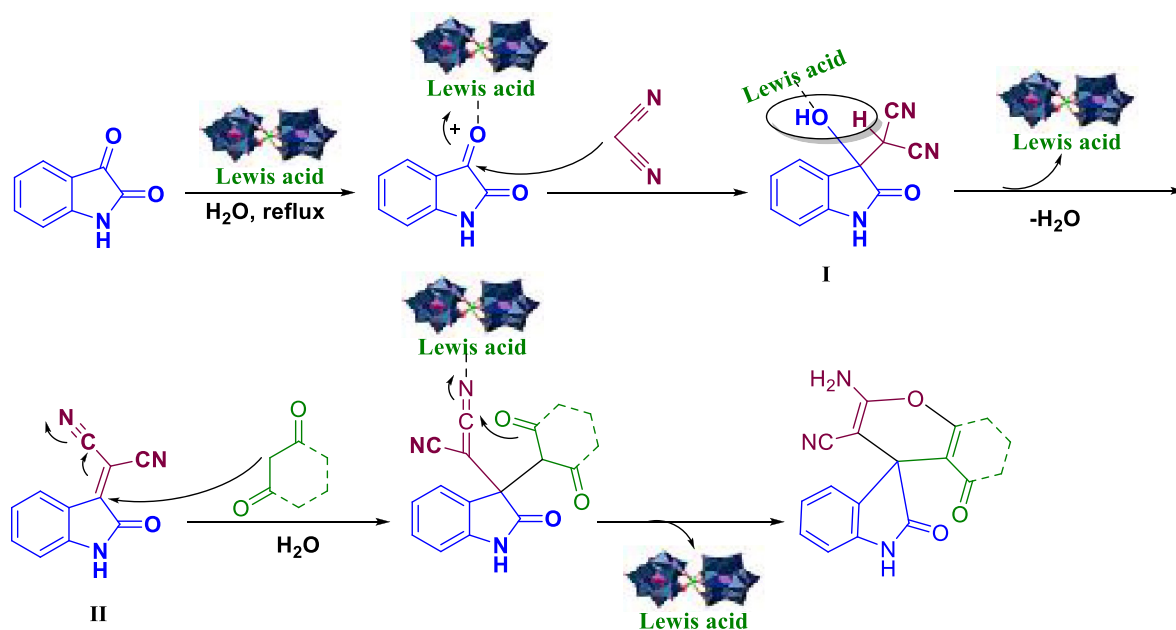
Entry	Product	Time (min)	Yield %	TOF	M.p./ °C Obs	M.p. °C/Lit
22		21	90	171	> 300	> 300
23		25	91	144	256–258	258–260
24		22	94	174	195–198	193–196
25		25	95	151	297–299	298–299
26		24	93	155	248–249	247–248

Table 3. Synthesis of spiro-2-amino-4H-pryans³⁷.



Scheme 1. The reasonable mechanism for the synthesis of spirooxindole derivatives.

Catalyst recyclability. Heterogeneous Catalysts, play an important and effective role in industries and other applications in laboratory scale. Hence, recyclability of the catalyst to prevent waste generation is one of the most important factors in catalysis. Nevertheless, recoverability of nano- $\text{Gd-B}_2\text{W}_{22}$ was evaluated on the model reaction and it was recycled up to 6 runs by simple filtration with a gradual decrease in activity from 96 to 85% in the corresponding product (Fig. 10). In addition, to elucidate whether the recycling process can result in any change in the catalyst's morphology and structure, the SEM image as well as FTIR spectra of the recycled nano- $\text{Gd-B}_2\text{W}_{22}$ catalyst were recorded (Fig. 11). These results support that the structure of the nano- $\text{Gd-B}_2\text{W}_{22}$ underwent several reactions was preserved, but some agglomeration is evident.

Concluding remarks

In the present study, a series of isostructural lanthanoid-containing polyoxometalate nanocatalysts $\text{Ln-B}_2\text{W}_{22}$ ($\text{Ln} = \text{La}, \text{Ce}, \text{Nd}, \text{Sm}, \text{Gd}, \text{and Er}$) were synthesized and characterized using a suite of analytical techniques. Among these nanocatalysts, the gadolinium-containing POM ($\text{Gd-B}_2\text{W}_{22}$) showed remarkable catalytic performance for the synthesis of bioactive isatin derivatives including spiro-2-amino-4H-pyrans, uracil fused spirooxindoles, and pyrroloacridine derivatives under the reflux condition in high yields and short reaction times (8–26 min). Also, further studies are underway in our laboratory to extend the application of these family nanocatalysts to other coupling reactions.

7a, 1.5h, 94%	7b, 2h, 90%	7c, 1.5h, 94%
TOF= 76	TOF= 57	TOF= 79
7d, 2h, 93%	7e, 1.5h, 94%	7f, 1.5h, 95%
TOF= 59	TOF= 79	TOF= 80
7g, 1h, 93%	7h, 1.5, 94%	7i, 2h, 95%
TOF= 116	TOF= 79	TOF= 60

Table 4. Synthesis of uracil-fused spirooxindoles^{10,38,39}.

<p>10a, 15min, 93 %</p>	<p>10b, 10 min, 91 %</p>	<p>10c, 10 min, 91 %</p>
TOF= 245	TOF= 356	TOF= 356
M.P.=195-197	M.P.=194-196	M.P.=188-190
<p>10d, 10 min, 94 %</p>	<p>10e, 12 min, 91 %</p>	<p>10f, 10 min, 91 %</p>
TOF= 368	TOF= 303	TOF= 356
M.P.=191-193	M.P.=202-204	M.P.=180-182
<p>10g, 16 min, 92 %</p>	<p>10h, 10 min, 92 %</p>	<p>10i, 15 min, 96 %</p>
TOF= 227	TOF= 360	TOF= 256
M.P.=222-224	M.P.=184-186	M.P.=178-181

Table 5. One-pot, three-component synthesis of pyrrolo[2,3,4-k]acridin-1-one derivatives^{45,46}.

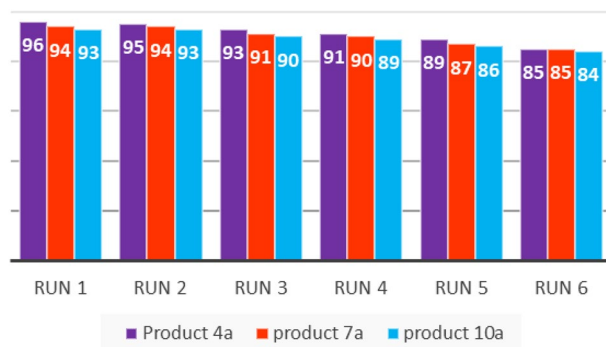


Figure 10. Reusability of nano-Gd-B₂W₂₂.

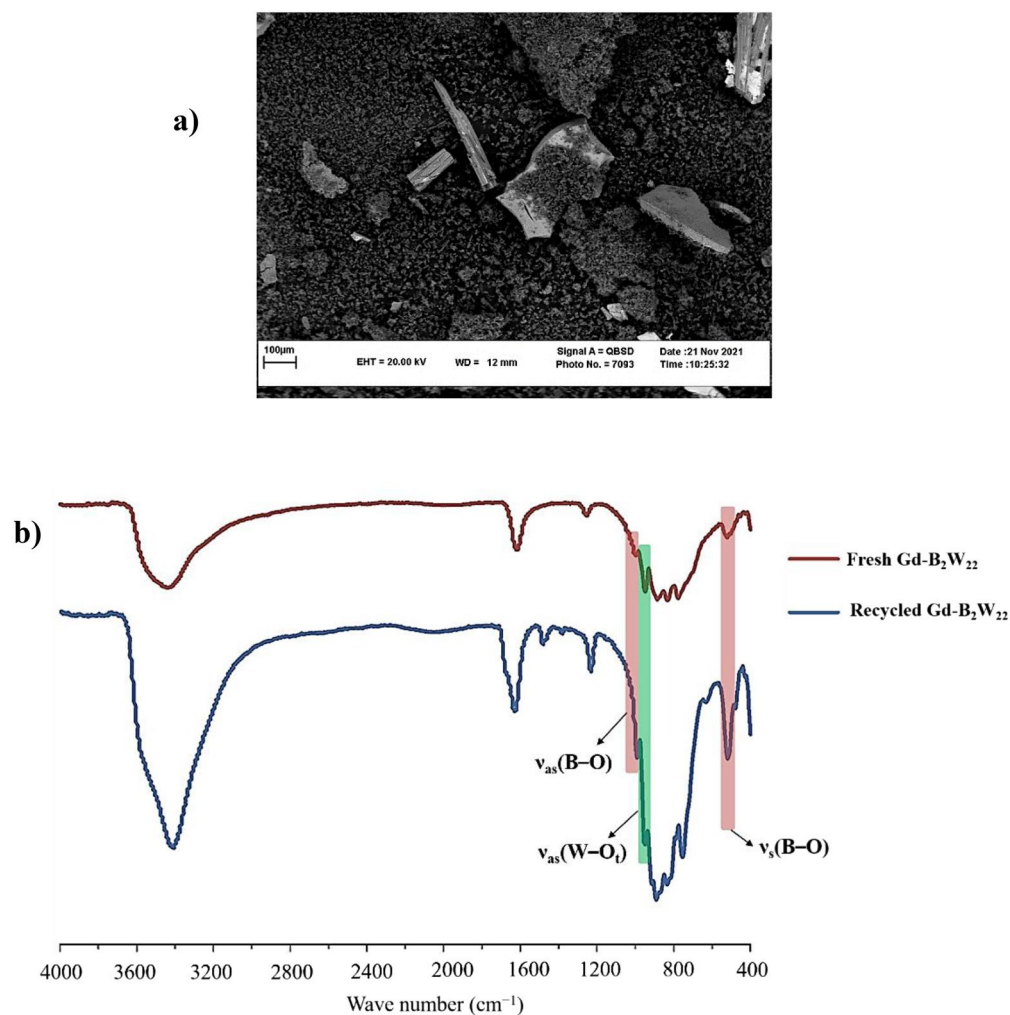


Figure 11. (a) SEM image of recycled nano-Gd-B₂W₂₂; (b) FTIR overlay of the fresh and recycled nano-Gd-B₂W₂₂.

Data availability

The raw/processed data that supports the findings of this study is available from the corresponding authors upon reasonable request.

Received: 8 January 2022; Accepted: 8 July 2022

Published online: 14 July 2022

References

- Rios, R. Enantioselective methodologies for the synthesis of spiro compounds. *Chem. Soc. Rev.* **41**, 1060–1074. <https://doi.org/10.1039/C1CS15156H> (2012).
- Ding, A., Meazza, M., Guo, H., Yang, J. W. & Rios, R. New development in the enantioselective synthesis of spiro compounds. *Chem. Soc. Rev.* **47**, 5946–5996. <https://doi.org/10.1039/C6CS00825A> (2018).
- Baeyer, A. Systematik und Nomenclatur bicyclischer Kohlenwasserstoffe. *Ber. Dtsch. Chem. Gesellschaft.* **33**, 3771–3775. <https://doi.org/10.1002/cber.190003303187> (1900).
- Saraswat, P., Jeyabalan, G., Hassan, M. Z., Rahman, M. U. & Nyola, N. K. Review of synthesis and various biological activities of spiro heterocyclic compounds comprising oxindole and pyrrolidine moieties. *Synth. Commun.* **46**, 1643–1664. <https://doi.org/10.1080/00397911.2016.1211704> (2016).
- Khafagy, M. M., Abd El-Wahab, A. H., Eid, F. A. & El-Agrody, A. M. Synthesis of halogen derivatives of benzo[h]chromene and benzo[a]anthracene with promising antimicrobial activities. *Farm.* **57**, 715–722. [https://doi.org/10.1016/S0014-827X\(02\)01263-6](https://doi.org/10.1016/S0014-827X(02)01263-6) (2002).
- Kornet, M. J. & Thio, A. P. Oxindole-3-spiropyrrolidines and -piperidines. Synthesis and local anesthetic activity. *J. Med. Chem.* **19**, 892–898. <https://doi.org/10.1021/jm00229a007> (1976).
- Abdel-Rahman, A. H., Keshk, E. M., Hanna, M. A. & El-Bady, S. M. Synthesis and evaluation of some new spiro indoline-based heterocycles as potentially active antimicrobial agents. *Bioorg. Med. Chem.* **12**, 2483–2488. <https://doi.org/10.1016/j.bmc.2003.10.063> (2004).
- Okita, T. & Isobe, M. Synthesis of the pentacyclic intermediate for dynemicin A and unusual formation of spiro-oxindole ring. *Tetrahedron* **50**, 11143–11152. [https://doi.org/10.1016/S0040-4020\(01\)89417-5](https://doi.org/10.1016/S0040-4020(01)89417-5) (1994).
- Usui, T., Kondoh, M., Cui, C.-B., Mayumi, T. & Osada, H. Tryprostatin A, a specific and novel inhibitor of microtubule assembly. *Biochem. J.* **333**, 543–548. <https://doi.org/10.1042/bj3330543> (1998).
- Paul, S. & Das, A. R. Dual role of the polymer supported catalyst PEG-OSO₃H in aqueous reaction medium: Synthesis of highly substituted structurally diversified coumarin and uracil fused spirooxindoles. *Tetrahedron Lett.* **54**, 1149–1154. <https://doi.org/10.1016/j.tetlet.2012.12.079> (2013).
- Maheshwar Rao, B. *et al.* Carbon–SO₃H: A novel and recyclable solid acid catalyst for the synthesis of spiro[4H-pyran-3,3'-oxindoles]. *Tetrahedron Lett.* **54**, 2466–2471. <https://doi.org/10.1016/j.tetlet.2013.02.089> (2013).
- Yang, P. & Korts, U. Discovery and evolution of polyoxopalladates. *Acc. Chem. Res.* **51**, 1599–1608. <https://doi.org/10.1021/acs.accounts.8b00082> (2018).
- Mirzaei, M., Eshtiagh-hosseini, H., Alipour, M. & Frontera, A. Recent developments in the crystal engineering of diverse coordination modes (0–12) for Keggin-type polyoxometalates in hybrid inorganic–organic architectures. *Coord. Chem. Rev.* **275**, 1–18. <https://doi.org/10.1016/j.ccr.2014.03.012> (2014).
- Taleghani, S., Mirzaei, M., Eshtiagh-hosseini, H. & Frontera, A. Tuning the topology of hybrid inorganic–organic materials based on the study of flexible ligands and negative charge of polyoxometalates: A crystal engineering perspective. *Coord. Chem. Rev.* **309**, 84–106. <https://doi.org/10.1016/j.ccr.2015.10.004> (2016).
- Herrmann, S., Ritchie, C. & Streb, C. Polyoxometalate–conductive polymer composites for energy conversion, energy storage and nanostructured sensors. *Dalton Trans.* **44**, 7092–7104. <https://doi.org/10.1039/C4DT03763D> (2015).
- Derakhshanrad, S., Mirzaei, M., Streb, C., Amiri, A. & Ritchie, C. Polyoxometalate-based frameworks as adsorbents for drug of abuse extraction from hair samples. *Inorg. Chem.* **60**, 1472–1479. <https://doi.org/10.1021/acs.inorgchem.0c02769> (2021).
- Alkbari, M., Mirzaei, M. & Amiri, A. Synergistic effect of lacunary polyoxotungstates and carbon nanotubes for extraction of organophosphorus pesticides. *Microchem. J.* **170**, 106665. <https://doi.org/10.1016/j.microc.2021.106665> (2021).
- Arab Fashapoyeh, M. *et al.* Photochemical and electrochemical hydrogen evolution reactivity of lanthanide-functionalized polyoxotungstates. *Chem. Commun.* **54**, 10427–10430. <https://doi.org/10.1039/C8CC06334F> (2018).
- Heravi, M. M. *et al.* H 5 BW 12 O 40 as a green and efficient homogeneous but recyclable catalyst in the synthesis of 4 H -Pyrans via multicomponent reaction. *Appl. Organomet. Chem.* **32**, e4479. <https://doi.org/10.1002/aoc.4479> (2018).
- Tamimi, M. *et al.* Ag 3 [PMo 12 O 40]: An efficient and green catalyst for the synthesis of highly functionalized pyran-annulated heterocycles via multicomponent reaction. *Appl. Organomet. Chem.* <https://doi.org/10.1002/aoc.5043> (2019).
- Babaei Zarch, M. *et al.* Single-molecule magnets within polyoxometalate-based frameworks. *Dalton Trans.* **50**, 15047–15056. <https://doi.org/10.1039/D1DT01708J> (2021).
- Coronado, E., Giménez-Saiz, C. & Gómez-García, C. J. Recent advances in polyoxometalate-containing molecular conductors. *Coord. Chem. Rev.* **249**, 1776–1796. <https://doi.org/10.1016/j.ccr.2005.02.017> (2005).
- Walsh, J. J., Bond, A. M., Forster, R. J. & Keyes, T. E. Hybrid polyoxometalate materials for photo(electro-) chemical applications. *Coord. Chem. Rev.* **306**, 217–234. <https://doi.org/10.1016/j.ccr.2015.06.016> (2016).
- Zhou, C., Li, S., Zhu, W., Pang, H. & Ma, H. A sensor of a polyoxometalate and Au-Pd alloy for simultaneously detection of dopamine and ascorbic acid. *Electrochim. Acta* **113**, 454–463. <https://doi.org/10.1016/j.electacta.2013.09.109> (2013).
- Arefian, M., Mirzaei, M., Eshtiagh-Hosseini, H. & Frontera, A. A survey of the different roles of polyoxometalates in their interaction with amino acids, peptides and proteins. *Dalton Trans.* **46**, 6812–6829. <https://doi.org/10.1039/C7DT00894E> (2017).
- Jia, Q., Cao, J., Duan, Y. & Hu, C. The solution chemistry and reactivity of lacunary Keggin silicotungstates monitored in real-time by a combination of mass spectrometry and electrochemistry. *Dalton Trans.* **44**, 553–559. <https://doi.org/10.1039/C4DT02723J> (2015).
- Patel, A., Narkhede, N., Singh, S. & Pathan, S. Keggin-type lacunary and transition metal substituted polyoxometalates as heterogeneous catalysts: A recent progress. *Catal. Rev.* **58**, 337–370. <https://doi.org/10.1080/01614940.2016.1171606> (2016).
- Lu, Y. *et al.* New polyoxometalate compounds built up of lacunary Wells–Dawson anions and trivalent lanthanide cations. *Inorg. Chem.* **45**, 2055–2060. <https://doi.org/10.1021/ic0515857> (2006).
- Yekke-Ghasemi, Z. *et al.* Fabrication of heterogeneous-based lacunary polyoxometalates as efficient catalysts for the multicomponent and clean synthesis of pyrazolopyranopyrimidines. *Inorg. Chem. Commun.* **140**, 109456. <https://doi.org/10.1016/j.inoche.2022.109456> (2022).
- Nie, Y.-M., Li, S.-H., Lin, M.-Y. & Yan, J. A micro-environment tuning approach for enhancing the catalytic capabilities of lanthanide containing polyoxometalate in the cyanosilylation of ketones. *Chem. Commun.* **56**, 3809–3812. <https://doi.org/10.1039/D0CC01216E> (2020).
- Narkhede, N., Singh, S. & Patel, A. Recent progress on supported polyoxometalates for biodiesel synthesis via esterification and transesterification. *Green Chem.* **17**, 89–107. <https://doi.org/10.1039/C4GC01743A> (2015).
- Lotfian, N., Heravi, M. M., Mirzaei, M. & Daraie, M. Investigation of the uncommon basic properties of [Ln(W₅O₁₈)₂]⁹⁻ (Ln = La, Ce, Nd, Gd, Tb) by changing central lanthanoids in the syntheses of pyrazolopyranopyrimidines. *J. Mol. Struct.* **1199**, 126953. <https://doi.org/10.1016/j.molstruc.2019.126953> (2020).
- Pradhan, S. & Mishra, B. G. Cs₃H₃-xPW₁₂O₄₀ nanoparticles dispersed in the porous network of Zr-pillared α-zirconium phosphate as efficient heterogeneous catalyst for synthesis of spirooxindoles. *Mol. Catal.* **446**, 58–71. <https://doi.org/10.1016/j.mcat.2017.12.013> (2018).
- Sadjadi, S., Heravi, M. M., Malmir, M. & Masoumi, B. HPA decorated Halloysite Nanoclay: An efficient catalyst for the green synthesis of Spirooxindole derivatives. *Appl. Organomet. Chem.* **32**, e4113. <https://doi.org/10.1002/aoc.4113> (2018).

35. Heravi, M. M., Momeni, T., Mirzaei, M., Zadsirjan, V. & Tahmasebi, M. An amino acid@isopolyoxometalate nanoparticles catalyst containing aspartic acid and octamolybdate for the synthesis of functionalized spirochromenes. *Inorg. Nano Metal Chem.* **51**, 896–909. <https://doi.org/10.1080/24701556.2020.1813172> (2021).
36. Nazish, M. *et al.* Magnetic Fe₃O₄ nanoparticle-supported phosphotungstic acid as a recyclable catalyst for the Kabachnik–Fields reaction of isatins, imines, and aldehydes under solvent-free conditions. *ChemPlusChem* <https://doi.org/10.1002/cplu.201402191> (2014).
37. Daraie, M., Beheshtiha, Y. S. & Heravi, M. M. Synthesis of spirochromene derivatives catalyzed by Mn(bpyo)₂/MCM-41 in water. *Monatshefte Chem. Chem. Mon.* **146**, 191–198. <https://doi.org/10.1007/s00706-014-1292-8> (2015).
38. Kavyani, S. & Baharfard, R. Design and characterization of Fe₃O₄/GO/Au–Ag nanocomposite as an efficient catalyst for the green synthesis of spirooxindole–dihydropyridines. *Appl. Organomet. Chem.* **34**, e5560. <https://doi.org/10.1002/aoc.5560> (2020).
39. Abdelmoniem, A. M., Hassaneen, H. M. E. & Abdelhamid, I. A. An efficient one-pot synthesis of novel spiro cyclic 2-oxindole derivatives of pyrimido[4,5-b]quinoline, pyrido[2,3-d:6,5-d']dipyrimidine and indeno[2',1':5,6]pyrido[2,3-d]pyrimidine in water. *J. Heterocycl. Chem.* **53**, 2084–2090. <https://doi.org/10.1002/jhet.2480> (2016).
40. Mougharbel, A. S. *et al.* Lanthanide-containing 22-tungsto-2-germanates [Ln(GeW₁₁O₃₉)₂] 13–: Synthesis, structure, and magnetic properties. *Inorg. Chem.* **59**, 4340–4348. <https://doi.org/10.1021/acs.inorgchem.9b03271> (2020).
41. Tézé, A., Michelon, M. & Hervé, G. Syntheses and structures of the tungstoborate anions. *Inorg. Chem.* **36**, 505–509. <https://doi.org/10.1021/ic961051t> (1997).
42. Bassil, B. S., Dickman, M. H., von der Kammer, B. & Kortz, U. The monolanthanide-containing silicotungstates [Ln(β-SiW₁₁O₃₉)₂]13 - (Ln = La, Ce, Sm, Eu, Gd, Tb, Yb, Lu): A synthetic and structural investigation. *Inorg. Chem.* **46**, 2452–2458. <https://doi.org/10.1021/ic061737d> (2007).
43. Arun, S., Kumar, V., Naz, A., Suhail, S. & Kumar, P. Journal of the Indian Chemical Society A comparative catalytic study using different metal ions by incorporating functionalized metallosalen into the lacunary position of Keggin polyoxometalate. *J. Indian Chem. Soc.* **98**, 100118. <https://doi.org/10.1016/j.jics.2021.100118> (2021).
44. Tsuruta, H., Imamoto, T. & Yamaguchi, K. Evaluation of the relative Lewis acidities of lanthanoid(III) compounds by tandem mass spectrometry. *Chem. Commun.* <https://doi.org/10.1039/a905569j> (1999).
45. Daraie, M., Lotfian, N., Heravi, M. M. & Mirzaei, M. Chemoselective synthesis of drug-like pyrrolo[2,3,4-kl]acridin-1-one using polyoxometalate@lanthanoid catalyst. *React. Kinet. Mech. Catal.* **129**, 391–401. <https://doi.org/10.1007/s11144-019-01709-3> (2020).
46. Kefayati, H., Narchin, F. & Rad-Moghadam, K. An unexpected multicomponent reaction leading to 2-arylpyrrolo[2,3,4-kl]acridin-1(2H)-ones. *Tetrahedron Lett.* **53**, 4573–4575. <https://doi.org/10.1016/j.tetlet.2012.06.070> (2012).

Acknowledgements

M.M. gratefully acknowledges financial support from the Ferdowsi University of Mashhad, the Iran Science Elites Federation (ISEF), Zeolite and Porous Materials Committee of Iranian Chemical Society and the Iran National Science Foundation (INSF). This work is supported by Iran Science Elites Federation Grant No. M/98208, M/99397, and M/400230. Also, M.M.H. acknowledges financially supported by Alzahra University, Tehran, Iran.

Author contributions

M.D.: Methodology, Formal analysis, Investigation, Software, Data curation, Writing–original draft preparation. M.M.: Conceptualization, Funding acquisition, Supervision, Main idea, Writing–review and editing, Project administration, Visualization. M.B.: Methodology, Formal analysis, Investigation, Software, Data curation, Writing–original draft preparation. V.S.A.: Experimental work. B.A.S.: Experimental work. M.M.H.: Conceptualization, Funding acquisition, Supervision, Main idea, Writing–review and editing, Project administration, Visualization.

Competing interests

The authors declare no competing interests.

Additional information

Supplementary Information The online version contains supplementary material available at <https://doi.org/10.1038/s41598-022-16384-z>.

Correspondence and requests for materials should be addressed to M.M. or M.M.H.

Reprints and permissions information is available at www.nature.com/reprints.

Publisher's note Springer Nature remains neutral with regard to jurisdictional claims in published maps and institutional affiliations.



Open Access This article is licensed under a Creative Commons Attribution 4.0 International License, which permits use, sharing, adaptation, distribution and reproduction in any medium or format, as long as you give appropriate credit to the original author(s) and the source, provide a link to the Creative Commons licence, and indicate if changes were made. The images or other third party material in this article are included in the article's Creative Commons licence, unless indicated otherwise in a credit line to the material. If material is not included in the article's Creative Commons licence and your intended use is not permitted by statutory regulation or exceeds the permitted use, you will need to obtain permission directly from the copyright holder. To view a copy of this licence, visit <http://creativecommons.org/licenses/by/4.0/>.

© The Author(s) 2022